Noname manuscript No.
(will be inserted by the editor)

Simultaneous measurements of reactive scalar and velocity in a planar liquid jet with a second-order chemical reaction

Tomoaki Watanabe · Yasuhiko Sakai · Kouji Nagata · Osamu Terashima · Takashi Kubo

Received: date / Accepted: date

https://doi.org/10.1007/s00348-012-1365-6

Abstract This paper presents a new experimental approach for simultaneous measurements of velocity and concentration in a turbulent liquid flow with a chemical reaction. For the simultaneous measurements, we developed a combined probe consisting of an I-type hot-film probe and an optical fiber probe based on the light absorption spectrometric method. In a turbulent planar liquid jet with a second-order chemical reaction ($A + B \rightarrow R$), streamwise velocity and concentrations of all reactive species are measured by the combined probe. The turbulent mass fluxes of the reactive species are estimated from the simultaneous measurements. The results show that the influence of the chemical reaction on the turbulent mass flux of the reactant species near the jet exit is different from its influence in other regions, and the turbulent mass flux of the product species has a negative value near the jet exit and a positive value in other regions.

Keywords Turbulent flow · Diffusion · Chemical reaction · Jet

Tomoaki Watanabe · Yasuhiko Sakai · Kouji Nagata · Osamu Terashima
Department of Mechanical Science and Engineering, Nagoya University, Nagoya 464-8603, Japan
Tel.: +81-52-789-4487
E-mail: watanabe.tomoaki@c.nagoya-u.jp
Takashi Kubo
Department of Mechanical Engineering, Meijo University, Nagoya 468-8502, Japan

1 Introduction

Turbulent diffusion involving chemical reactions is important in various scientific fields. From an engineering point of view, we are concerned with predictions of pollutant emission and designs of combustors and chemical reactors. It is critical to elucidate the mechanism of chemical reaction in turbulence.

To investigate the mixing process, dispersion, and chemical reaction in a turbulent flow in detail, information on the velocity field as well as the scalar field is indispensable. Hence, in experiments, it is useful to measure instantaneous velocity and instantaneous concentrations of multiple species simultaneously in a turbulent flow.

In a gas phase, Su and Mungal (2004) have measured two-component velocities and concentration by combining planar laser induced fluorescence method (PLIF) with particle image velocimetry (PIV) in a non reactive jet. In reactive gas flows, Bilger et al. (1991), Brown and Bilger (1996), and Li and Bilger (1996) have performed simultaneous measurements of velocity and concentration of reactive species by using hot-wire anemometry and chemiluminescent analyzers.

In a liquid phase, the Batchelor scale, which is the smallest scale of scalar fluctuation, is smaller than the Kolmogorov length scale, which is the smallest length scale of the velocity fluctuation, because of high Schmidt number. Hence, the experiment in a turbulent liquid flow is more difficult to conduct than that in a gas flow. In non reactive liquid jets, Sakai et al. (1999) have simultaneously measured the velocity and concentration by combining an I-type hot-film anemometry with light absorption spectrometry, and Webster et al. (2001) have simultaneously measured two-component velocities and concentration by combining PLIF with particle tracking velocimetry (PTV). PLIF and PIV have been also used for the simultaneous measurements of two-component velocities and concentration in non reactive liquid flows by some researchers (e.g. Borg et al. 2001, Hu et al. 2004, Feng et al. 2007, and Feng et al. 2010).

In reactive liquid flows, measurements of instantaneous concentration of reactive species have been carried out in grid turbulence (Bennani et al. 1985; Mehta and Tarbell 1987; Komori et al. 1994) and in a planar jet (Kubo et al. 2009). However, few previous experiments (e.g., Komori et al. 1993) have simultaneously measured the velocity and concentration of reactive species in a reacting liquid flow.

In this study, we developed a combined probe for simultaneous measurements of velocity and concentrations of reactive species in a liquid phase. The combined probe consists of an I-type hot-film anemometer and an optical fiber probe based on the light absorption spectrometric method (Lee and Brodkey 1964; Nakamura et al. 1987). Although this measurement method is invasive and the two probes comprising the combined probe are slightly separated from each another, it is confirmed that reliable data are obtained by this method. We applied this method to the simultaneous measurement in a planar liquid jet with a second-order chemical reaction.

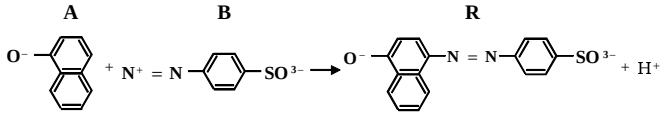

Fig. 1 Details of the chemical reaction.

2 Experiments

2.1 Chemical reaction

The chemical reaction investigated in this study is the first reaction of the series-parallel reactions and is given by

$$\mathrm{A} + \mathrm{B} \rightarrow \mathrm{R}. \tag{1}$$

The reactants are 1-naphthol (A) and diazotized sulfanilic acid (B), and the product is 4-(4′-sulphophenylazo)-1-naphthol (R), briefly referred to as monoazo dyestuff. Figure 1 shows the details of the chemical reaction. The basic properties of series-parallel reactions have been investigated thoroughly (Bourne et al. 1985). This is a second-order reaction and the reaction rate constant of the first reaction is $k = 12,000$ m^3/(mol· s) under the present experimental condition.

A water solution of species A is issued into the main stream containing species B as a planar jet. This reaction has a pH dependency. To keep the pH constant, sodium carbonate and sodium hydrogen carbonate are added into the jet flow as buffer salts. For simultaneous measurements of all reactive species based on conserved scalar theory, blue dyestuff (C: Acid Blue 9) is also added into the jet flow. The concentration of species C is considered as the conserved scalar and is independent of the chemical reaction. In this study, it was ascertained that species C is independent of the above chemical reaction. Since species R and C have light absorption characteristics, it is possible to measure the concentrations of these two species by light absorption spectrometry.

2.2 Experimental apparatus and conditions

Figure 2 shows the experimental apparatus. The main flow and the jet flow are supplied to the test section through the head tank. The jet flow involving species A and C is ejected into the main flow from a rectangular slit with a width of 2 mm and a length of 40 mm. The cross section of the test section is rectangular with a width of 160 mm and a length of 40 mm, and the height of the test section is 300 mm. The details of the test section are shown in Fig. 3. The streamwise and cross-stream directions are represented by x and y, respectively. The origin of the coordinate system is located at the median point

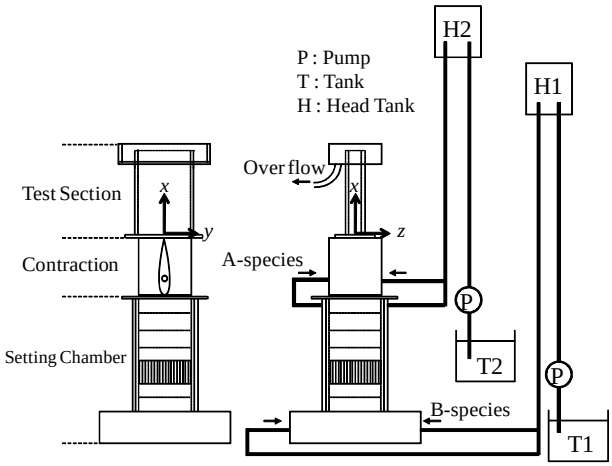

Fig. 2 Experimental apparatus.

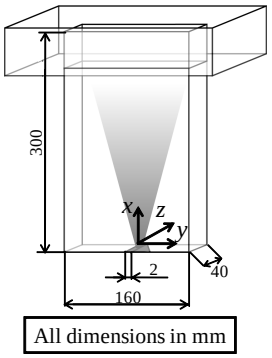

Fig. 3 Test section.

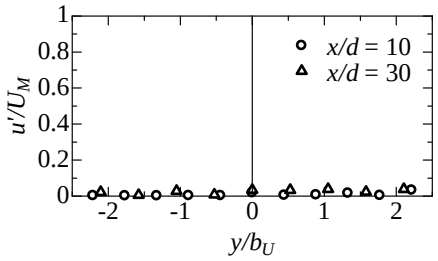

Fig. 4 Transverse profiles of turbulent intensity in the main flow.

of the slit through which the jet flow is ejected. The streamwise mean velocity of the main flow is $U_M = 0.073$ m/s and the mean velocity of the jet flow at the slit exit is $U_J = 1.29$ m/s. The Reynolds number, $Re = (U_J - U_M)d/\nu$, is 2,200. Here, d is the slit width and ν is the kinematic viscosity. The initial concentrations of reactive species A and B, denoted by Γ_{A0} and Γ_{B0}, are set to 0.4 and 0.2 mol/m^3, respectively, and the initial concentration of non reactive species C, Γ_{C0}, is 0.1 kg/m^3. The Damköhler number, $Da = k(\Gamma_{A0} + \Gamma_{B0})d/(U_J - U_M)$, is 11.8. To measure background level of turbulent velocity in the main flow, turbulent intensity u'/U_M was measured by an I-type hot-film probe at $x/d = 10$ and 30 in the absence of the planar jet. Figure 4 shows the transverse profiles of turbulent intensity u'/U_M in the main flow. Here, u' is the rms value of the streamwise velocity fluctuation and b_U is the half-width of the mean streamwise velocity measured in the planar jet. Figure 4 shows that u' (i.e. background level of turbulent velocity) is much smaller than U_M.

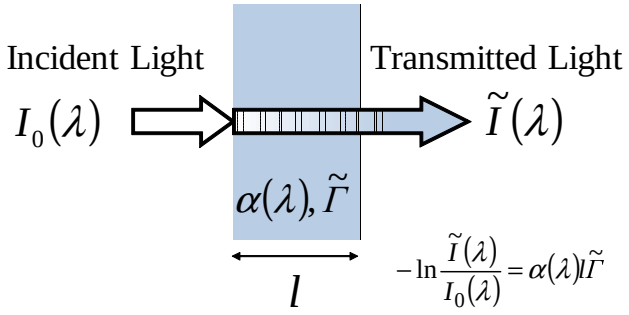

Fig. 5 Light absorption spectrometric method.

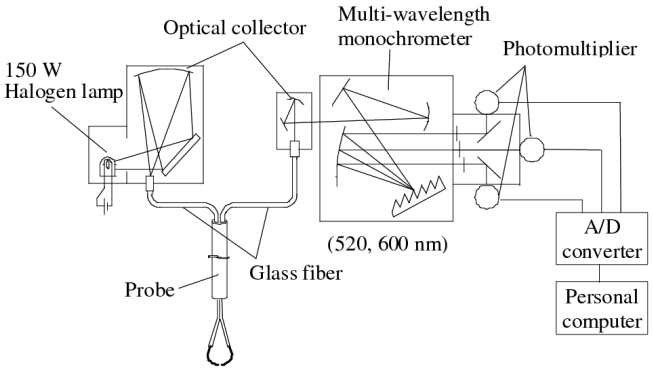

Fig. 6 Schematic of the optical system for the concentration measurement.

2.3 Concentration measurement method

An optical fiber probe based on light absorption spectrometry is used to measure instantaneous concentrations of species R and C. The details of the optical fiber probe have been presented in Nakamura et al. (1987). Assuming that light of wavelength λ passes through the solution of one absorptive species i (see Fig. 5), we can write the Beer's absorption law as

$$-\ln\frac{\tilde{I}(\lambda)}{I_0(\lambda)} = \alpha_i(\lambda) l \tilde{\Gamma}_i, \tag{2}$$

where $I_0(\lambda)$ is the intensity of incident light, $\tilde{I}(\lambda)$ is the instantaneous intensity of transmitted light, l is the length of the solution, $\tilde{\Gamma}_i$ is the instantaneous concentration of absorptive species i, and α_i is the function of λ and dependent on the light absorption characteristics of species i. Now, we introduce $\tilde{P}(\lambda)$ and $k_i(\lambda)$ defined as follows:

$$\tilde{P}(\lambda) = -\ln\frac{\tilde{I}(\lambda)}{I_0(\lambda)}, \tag{3}$$

$$k_i(\lambda) \quad = \alpha_i(\lambda) l. \tag{4}$$

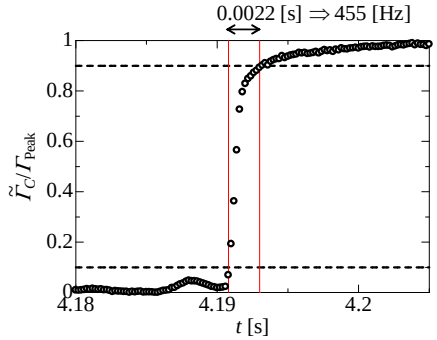

Fig. 7 Time series data of concentration.

$\tilde{P}(\lambda)$ and $k_i(\lambda)$ are here called the light absorption spectrum and the light absorption coefficient, respectively. Using Eq. (2), we can relate $\tilde{P}(\lambda)$ and $k_i(\lambda)$ by

$$\tilde{P}(\lambda) = k_i(\lambda)\tilde{\Gamma}_i. \tag{5}$$

$k_i(\lambda)$ is previously obtained by measuring $\tilde{P}(\lambda)$ for a solution whose concentration of species i is known, and, therefore, $\tilde{P}(\lambda)$ measured by the optical fiber probe can be converted into the instantaneous concentration by Eq. (5).

Now, we consider a solution of multiple absorptive species. $\tilde{P}(\lambda)$ for this solution is equal to the sum of each $\tilde{P}(\lambda)$ for the solution of one absorptive species. Specifically, we consider the solution of two absorptive species R and C. For light of wavelength λ_n, $\tilde{P}(\lambda_n)$ is written as

$$\tilde{P}(\lambda_n) = -\ln\frac{\tilde{I}(\lambda_n)}{I_0(\lambda_n)} = k_R(\lambda_n)\tilde{\Gamma}_R + k_C(\lambda_n)\tilde{\Gamma}_C. \tag{6}$$

Here, $k_C(\lambda_n)$ and $k_R(\lambda_n)$ for the solution of two absorptive species R and C are the same as $k_C(\lambda_n)$ and $k_R(\lambda_n)$ for the solution that involves one species R or C. Hence, concentration of two absorptive species is obtained from Eq. (6) and $\tilde{P}(\lambda_n)$ for two wavelengths if $k_i(\lambda_n)$ is investigated previously for two species and for two wavelengths.

The schematic of the optical system for concentration measurement is shown in Fig. 6, which is the same as used in Sakai et al. (1997). A halogen lamp is used as a multiwavelength light source. For the measurement of $\tilde{P}(\lambda)$ for two wavelengths, the halogen lamp light is split into two wavelengths (520 and 600 nm) by a prism spectroscope. The light intensity is measured by a photomultiplier. The core diameter of the optical fiber used in the optical fiber probe is 0.5 mm and the length of the sampling volume of the optical fiber probe is 0.7 mm.

The frequency response of the concentration measurement system is important to detect concentration fluctuations in a turbulent flow. In this study, two methods are used to estimate the frequency response of the concentration measurement system.

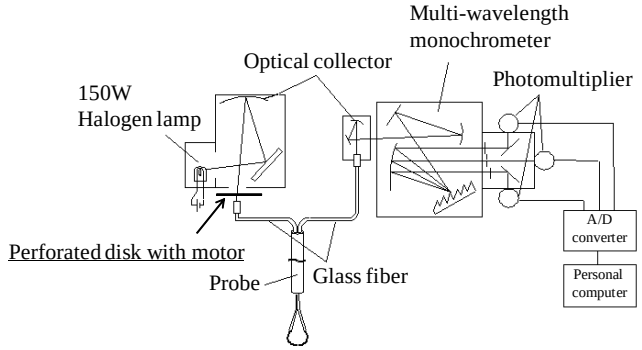

Fig. 8 Schematic of the optical system for frequency response test.

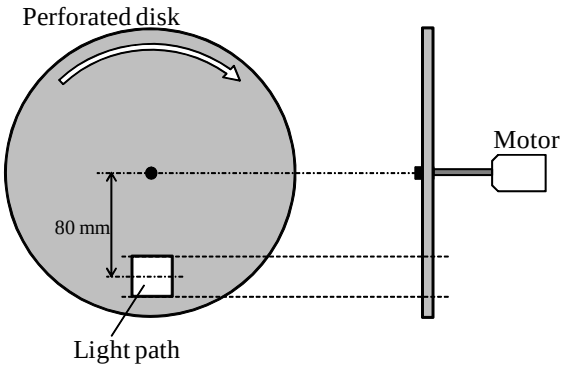

Fig. 9 The perforated disk with the motor.

First, according to Madhani and Brown (2008), we try to estimate the frequency response. The optical fiber probe is put at the jet exit, and then solution of non reactive species C is ejected at the velocity of 1.29 m/s. Time series data of $\tilde{\Gamma}_C$ is measured by the concentration probe, and typical experimental data is shown in Fig. 7. In Fig. 7, $\tilde{\Gamma}_C$ is normalized by the peak concentration Γ_{Peak}. Figure 7 also shows the frequency response estimated from a rise time according to Madhani and Brown (2008). This estimation shows the frequency response of 455 Hz. This method assumes that the concentration variation by the injection of dye can be regarded as the step function. However, in Fig. 7, $\tilde{\Gamma}_C/\Gamma_{\mathrm{Peak}}$ gradually increases from 0.9 to 1.0, and this implies that the concentration variation by the injection of dye cannot be approximated by the step function in our experiments because the interface between the solution and water is not completely flat due to the velocity disturbance in the test section and/or the molecular diffusion at the jet exit. Hence, the frequency response predicted by this approach may be lower than the actual value.

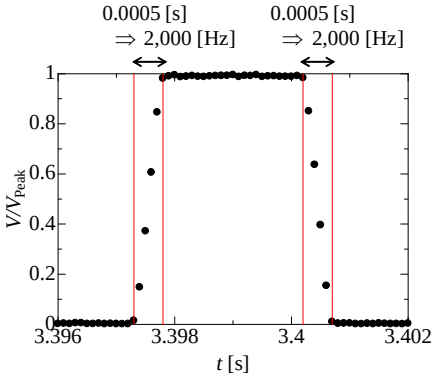

Fig. 10 Time series data of voltage.

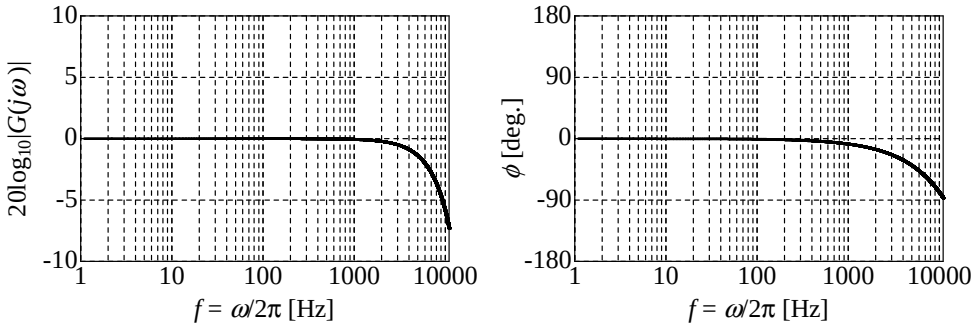

(a) Gain characteristics. (b) Phase characteristics.

Fig. 11 Frequency response test of concentration measurement system.

Figure 8 shows the schematic of the optical system for the second frequency response test. As shown in Fig. 8, a perforated disk with a motor, the detail of which is shown in Fig. 9, is newly installed on the concentration measurement system. The perforated disk with the motor has an open hole on the disk. The open hole acts as the light path. The motor has a rotating rate of 842 rpm. Because the open hole lies 80 mm away from the center of the disk, the open hole rotates with 7.05 m/s. The perforated disk passes the light when the open hole is on the light path of the measurement system, and otherwise, the perforated disk blocks the light. Thus, the role of the perforated disk varies according to the position of the open hole. By using the optical system shown in Fig. 8, we measure the signal from the photomultiplier. Figure 10 shows the typical time series data of voltage V normalized by the maximum value V_{Peak}. The frequency response can be estimated from the rise and fall response times of signals shown in Fig. 10, and this estimation shows the frequency response of 2,000 Hz. The same frequency responses are obtained from the rise and fall response times. The frequency response can also be obtained from the

transfer function defined by $G(s) = Y(s)/X(s)$. Here, $X(s)$ and $Y(s)$ are the Laplace transforms of input and output signals, respectively. The output signal is shown in Fig. 10, and the input signal is calculated from the rotation speed of the perforated disk and the diameter of the light which passes through the open hole of perforated disk. Figure 11 shows the gain and phase ($\phi = -\angle G(jf)$) characteristics of the concentration measurement system. Here, $j = \sqrt{-1}$. The frequency response estimated from Fig. 11 is about 3,000 Hz. These results show that the frequency response of the concentration measurement system is at least 2,000 Hz.

Instantaneous concentrations of absorptive species R and C are simultaneously measured by the optical fiber probe based on light absorption spectrometry. However, species A and B do not have light absorption characteristics. To determine the concentrations of species A and B, conserved scalar theory (Bilger et al. 1991) must be applied. According to conserved scalar theory, the instantaneous concentrations of species A and B are given by

$$\tilde{\Gamma}_A = \tilde{\xi}\Gamma_{A0} - \tilde{\Gamma}_R, \tag{7}$$
$$\tilde{\Gamma}_B = (1-\tilde{\xi})\Gamma_{B0} - \tilde{\Gamma}_R, \tag{8}$$

where Γ_{A0} and Γ_{B0} are the initial concentration of species A and B, respectively, and $\tilde{\xi}$ is called the mixture fraction, with the tilde ($\tilde{}$) denoting the instantaneous value. The mixture fraction is a conserved scalar and is not affected by the chemical reaction. In this study, the mixture fraction is defined by the normalized concentration of species C:

$$\tilde{\xi} = \tilde{\Gamma}_C/\Gamma_{C0}, \tag{9}$$

where Γ_{C0} is the initial concentration of species C. From Eqs. (7) and (8), the mass conservation law is derived as follows:

$$\frac{\tilde{\Gamma}_A}{\Gamma_{A0}} + \frac{\tilde{\Gamma}_B}{\Gamma_{B0}} + \frac{\tilde{\Gamma}_R}{\Gamma_{R0}} = 1, \tag{10}$$

where Γ_{R0} is defined as

$$\Gamma_{R0} = \frac{\Gamma_{A0}\Gamma_{B0}}{\Gamma_{A0} + \Gamma_{B0}}. \tag{11}$$

From Eqs. (7) and (8), for $k \to 0$, the frozen limit corresponding to the limiting case of no reaction is derived as follows:

$$\lim_{k\to 0} \tilde{\Gamma}_A = \tilde{\Gamma}_A^0 = \tilde{\xi}\Gamma_{A0}, \tag{12}$$
$$\lim_{k\to 0} \tilde{\Gamma}_B = \tilde{\Gamma}_B^0 = (1-\tilde{\xi})\Gamma_{B0}, \tag{13}$$
$$\lim_{k\to 0} \tilde{\Gamma}_R = \tilde{\Gamma}_R^0 = 0. \tag{14}$$

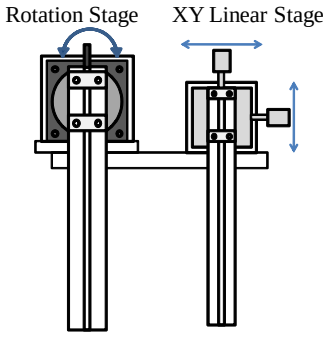

Fig. 12 The probe stage.

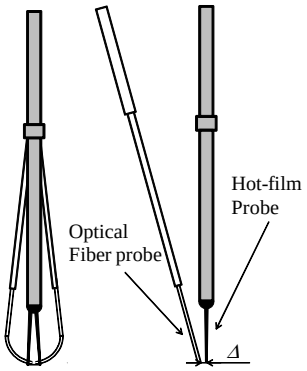

Fig. 13 The combined probe.

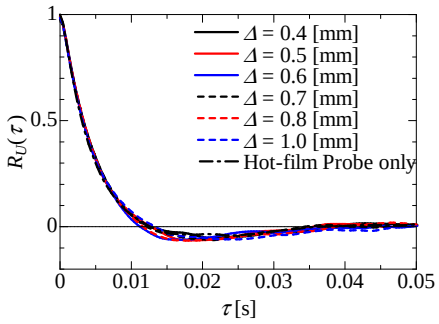

Fig. 14 Autocorrelation coefficient of velocity (Case A).

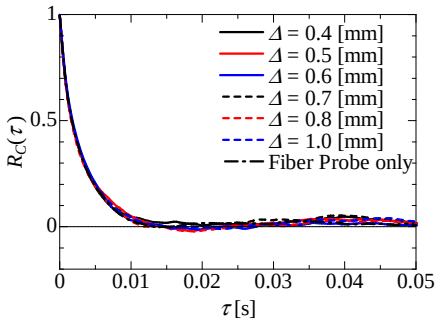

Fig. 15 Autocorrelation coefficient of concentration (Case B).

Furthermore, for $k \to \infty$, we can derive the equilibrium limit corresponding to the limiting case of the fast chemical reaction as follows;

$$\lim_{k\to\infty} \tilde{\Gamma}_A = \tilde{\Gamma}_A^{\infty} = (\Gamma_{A0} + \Gamma_{B0})(\tilde{\xi} - \xi_S)H(\tilde{\xi} - \xi_S), \tag{15}$$

$$\lim_{k\to\infty} \tilde{\Gamma}_B = \tilde{\Gamma}_B^{\infty} = (\Gamma_{A0} + \Gamma_{B0})(\xi_S - \tilde{\xi})H(\xi_S - \tilde{\xi}), \tag{16}$$

$$\lim_{k\to\infty} \tilde{\Gamma}_R = \tilde{\Gamma}_R^{\infty} = \Gamma_{B0}(1 - \tilde{\xi})H(\tilde{\xi} - \xi_S) + \Gamma_{A0}\tilde{\xi}H(\xi_S - \tilde{\xi}). \tag{17}$$

Here, $H(z)$ is the Heaviside step function and is equal to 0 for $z \leq 0$ or 1 for $z > 0$. ξ_S is the stoichiometric value of the mixture fraction and is given by $\xi_S = \Gamma_{B0}/(\Gamma_{A0} + \Gamma_{B0})$. In this study, $\xi_S = 0.333$.

2.4 The combined probe for simultaneous measurement

A combined probe, which consists of the I-type hot-film probe and the optical fiber probe, is developed for the simultaneous measurements of streamwise velocity and concentration. Figures 12 and 13 show the details of the combined

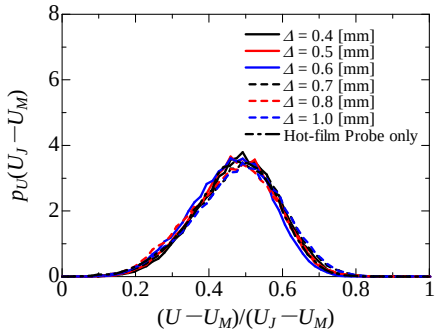

Fig. 16 Probability density function of velocity (Case A).

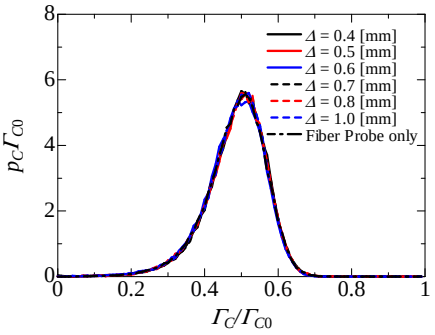

Fig. 17 Probability density function of concentration (Case B).

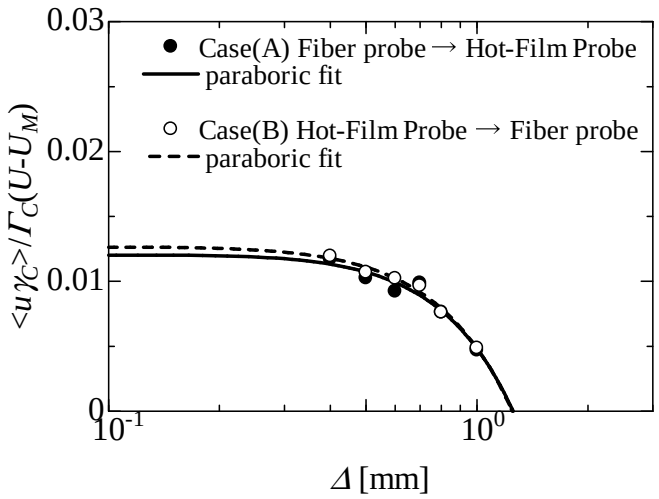

Fig. 18 Spatial correlation between velocity and concentration.

probe. The probe stage (Fig. 12) is used to hold the optical fiber probe and the hot-film probe. The optical fiber probe and the hot-film probe are set up on a rotary stage and an XY linear stage, respectively. Figure 13 shows the details of the combined probe. The distance Δ between the two probes (the optical fiber probe and the hot-film probe) is adjustable by using the XY linear stage on which the hot-film probe is fixed.

The validity of this combined probe is confirmed below. It is required that the probe distance Δ be small enough to measure concentration and velocity simultaneously, but in the case when the two probes are very close to each other, it is expected that one probe would interfere with the signal measured by the other probe. Hence, we investigated the influence of the probe distance on the measured signals. In the experiment, a water solution of species C is injected into the main stream as a planar jet and the concentration of species

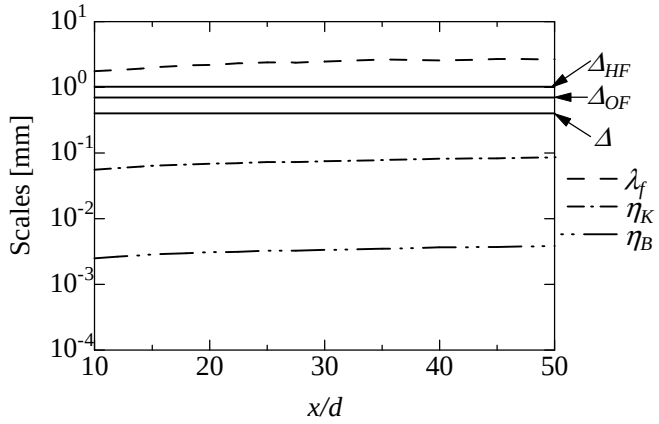

Fig. 19 The probe resolution and scales of the flow on the jet centerline.

C and the streamwise velocity are measured simultaneously at $x/d = 20$ on the centerline of the jet by the combined probe at distances $\Delta = 0.4$, 0.5, 0.6, 0.7, 0.8, and 1.0 mm. The minimum value of the probe distance $\Delta = 0.4$ mm is set to prevent the hot-film probe from damage by contact with the optical fiber probe. We investigated two cases: In case A the optical fiber probe is brought close to the hot-film probe fixed on the jet centerline, and in case B the hot-film probe is brought close to the optical fiber probe fixed on the jet centerline. First, to examine the influence of the small distance between the two probes on the measurement results, autocorrelation functions and probability density functions (PDFs) of the streamwise velocity and the concentration of species C are measured. Figures 14 and 15 show the autocorrelation functions of the streamwise velocity and the concentration of species C and Figs. 16 and 17 show the PDFs of the streamwise velocity and the concentration of species C. These figures also show the results separately measured by each probe. The results obtained by the combined probe almost coincide with the results from each separate probe, demonstrating that the two probes do not interfere with each other even for $\Delta = 0.4$ mm.

Then, to make sure that $\Delta = 0.4$ mm is small enough to simultaneously measure velocity and concentration, the spatial correlation $\langle u\gamma_C \rangle$ between the streamwise velocity fluctuation (u) and the concentration fluctuation of species C (γ_C) is measured at $\Delta = 0.4$, 0.5, 0.6, 0.7, 0.8, and 1.0 mm. Here, $\langle * \rangle$ denotes an ensemble average of $*$. Figure 18 shows the spatial correlation $\langle u\gamma_C \rangle$ normalized by the mean streamwise velocity difference $(U - U_M)$ and the mean concentration of species C (Γ_C). $\langle u\gamma_C \rangle$ is expected to be an even function of Δ, and decreases as the probe distance $|\Delta|$ becomes large. Therefore, it is reasonable to approximate $\langle u\gamma_C \rangle$ by a quadratic function of Δ. Fig. 18 also shows the quadratic curves obtained by the method of least squares. Assuming that the true value of the turbulent mass flux of concentration of species C is equal to the limiting value of these quadratic curves as $\Delta \to 0$, we can

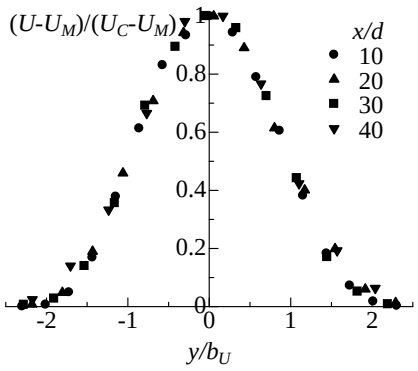

Fig. 20 Lateral profiles of the mean streamwise velocity.

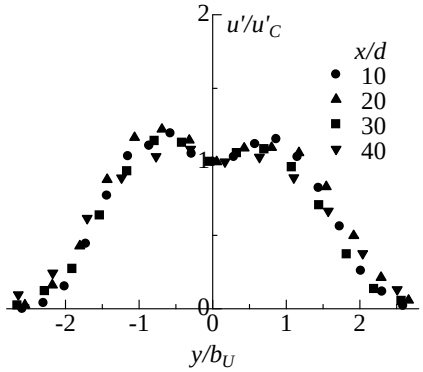

Fig. 21 Lateral profiles of the rms value of the streamwise velocity fluctuation.

estimate that the error of the turbulent mass flux measured by the combined probe ($\Delta = 0.4$ mm) is 4.7% for case A and 1.2% for case B. These results imply that when the distance between the two probes is set to 0.4 mm it is possible to measure velocity and concentration simultaneously using the combined probe.

The spatial resolution of the optical fiber probe, Δ_{OF}, is equal to the length of the sampling volume (0.7 mm) and the spatial resolution of the hot-film probe, Δ_{HF}, is equal to the length of the sensing element (1.02 mm). Note that the core diameter of the optical fiber probe is 0.5 mm, which is smaller than Δ_{OF}. Similarly, the diameter of the wire is 50.8 μm, which is smaller than Δ_{HF}. Here, we compare the values of Δ_{OF}, Δ_{HF}, Δ with the Kolmogorov scale η_K, the Batchelor scale η_B, and the Taylor microscale λ_f. We estimated η_K from $\eta_K = (\nu^3/\epsilon)^{1/4}$. Here, ϵ is the turbulent kinematic energy dissipation rate calculated by $\epsilon = 15\nu\langle(\partial u/\partial x)^2\rangle$. η_B is calculated from $\eta_B = \eta_K/Sc^{1/2}$, where Sc is the Schmidt number and $Sc \sim 500$ for the non reactive species C. λ_f is calculated from $\lambda_f = u'/\sqrt{\langle(\partial u/\partial x)^2\rangle}$ on the jet centerline. Figure 19 shows the axial variations of η_K, η_B, and λ_f. Figure 19 also shows the values of Δ_{OF}, Δ_{HF}, and Δ. From Fig. 19, it is found that the spatial resolution of the combined probe is smaller than λ_f.

3 Experimental Results

Figure 20 shows the lateral profiles of the mean streamwise velocity $(U - U_M)$ normalized by the centerline value $(U_C - U_M)$ and Fig. 21 shows the lateral profiles of the rms value of the streamwise velocity fluctuation normalized by the centerline value. Here, the prime ($'$) denotes the rms value. In Figs. 20 and 21, the abscissa is normalized by the velocity half-width b_U. Figures 22 and 23 show the lateral profiles of the mean mixture fraction ξ normalized by the centerline value ξ_C and the rms value ξ' of the mixture fraction fluctuation

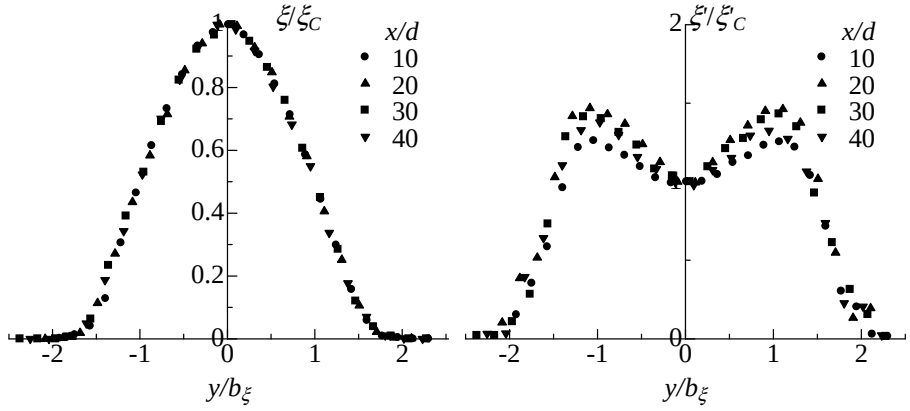

Fig. 22 Lateral profiles of the mean mixture fraction.

Fig. 23 Lateral profiles of the rms value of the mixture fraction fluctuation.

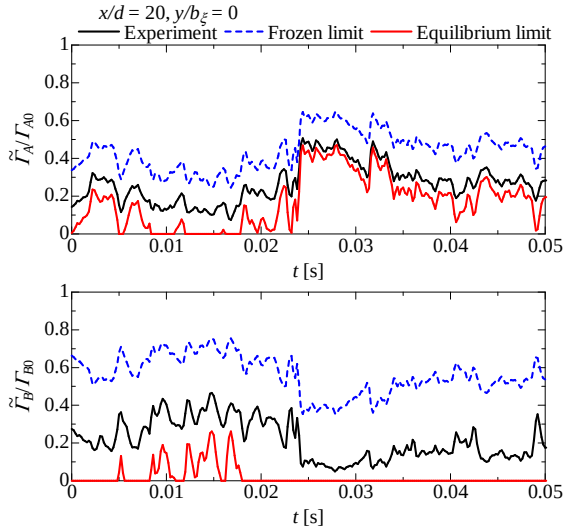

Fig. 24 Time series data of instantaneous concentration of reactant species A at $x/d = 10$ on the jet centerline.

normalized by the centerline value ξ'_C, respectively. Here, the abscissa is normalized by the half-width of the mixture fraction b_ξ. In Figs. 20–23 the lateral profiles of mean and rms streamwise velocities and mean and rms mixture fractions exhibit the good self-similarity.

Instantaneous concentrations of reactant species A and B ($\tilde{\Gamma}_A$ and $\tilde{\Gamma}_B$) are calculated from Eqs. (7) and (8). To accurately measure $\tilde{\Gamma}_A$ and $\tilde{\Gamma}_B$ from Eqs. (7) and (8), constant values of Γ_{A0} and Γ_{B0} are required. Namely, reactant species A and B must be homogeneously premixed. From the conserved scalar

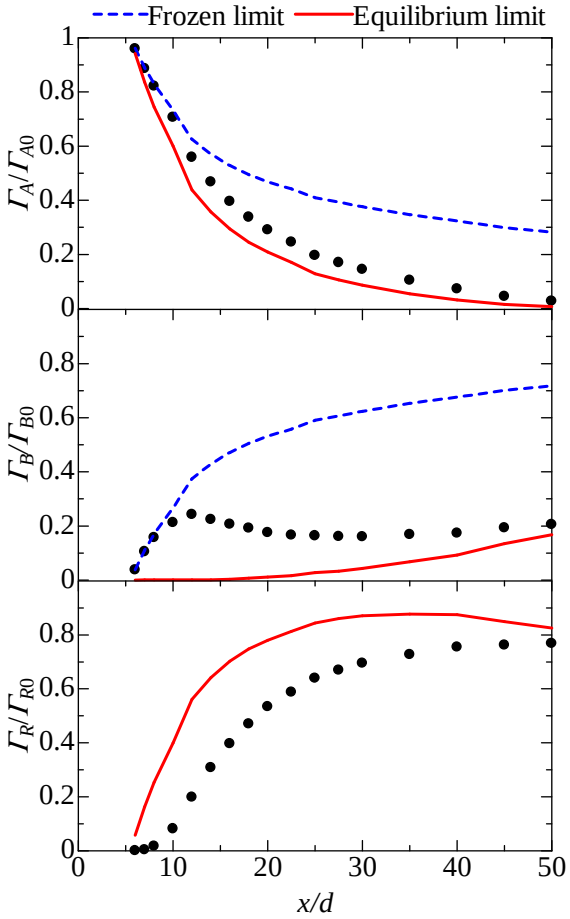

Fig. 25 The streamwise evolution of mean concentrations of reactive species.

theory, the following inequality can be derived;

$$\tilde{\Gamma}_\alpha^\infty \leq \tilde{\Gamma}_\alpha \leq \tilde{\Gamma}_\alpha^0. \tag{18}$$

Here, $\alpha = A$ or B. If Γ_{A0} and Γ_{B0} are not constant, $\tilde{\Gamma}_A$ and $\tilde{\Gamma}_B$ calculated from Eqs. (7) and (8) are expected not to satisfy the above inequality. Hence, by using this inequality, we can confirm whether $\tilde{\Gamma}_A$ and $\tilde{\Gamma}_B$ are accurately measured or not. Figure 24 shows the time series data of $\tilde{\Gamma}_A$ and $\tilde{\Gamma}_B$ at $x/d = 20$ on the jet centerline. Figure 24 also shows the concentrations for the frozen and equilibrium limits. In Fig. 24, the concentrations of reactant species A and B always lie between the concentrations for the frozen and equilibrium limits as expected from the conserved scalar theory (Bilger et al. 1991). The results imply that the measurements of concentrations of species A and B are accurately conducted by using the conserved scalar theory, and there are

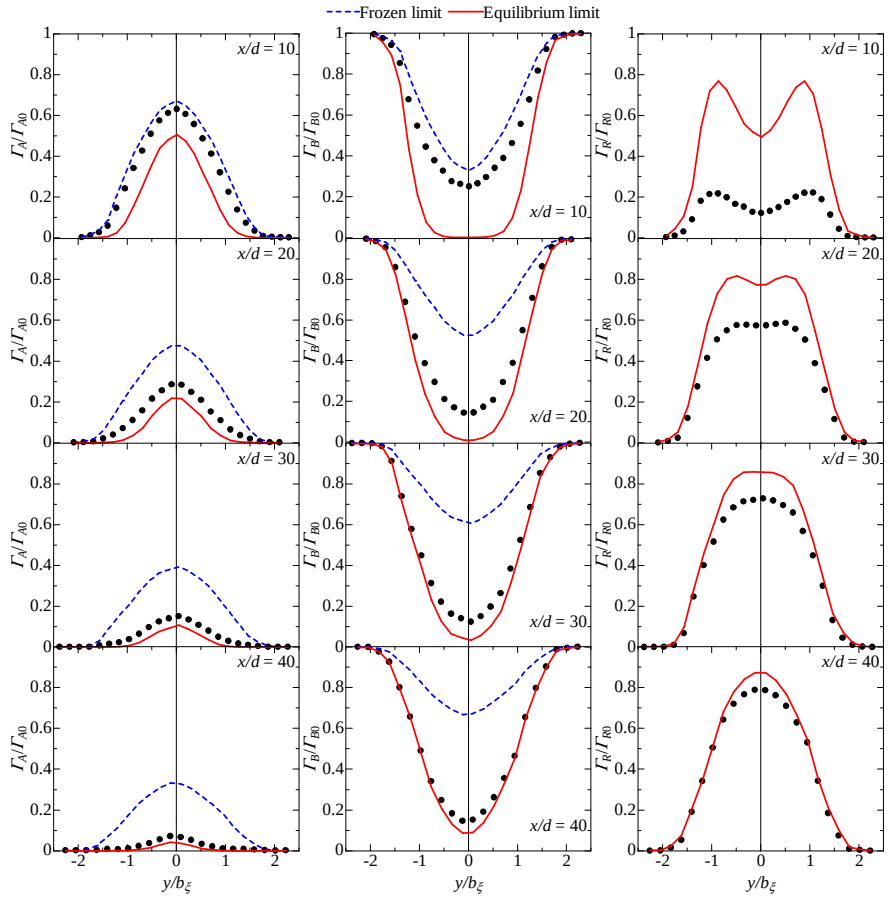

Fig. 26 Lateral profiles of the mean concentrations of reactive species.

no problems with the assumption of homogeneously mixed reactants which is used in the conserved scalar theory.

Figures 25 and 26 show the streamwise evolution and the lateral profiles of mean concentration of reactive species Γ_i (i = A, B, or R), respectively. Γ_A and Γ_B are normalized by the respective initial concentrations and Γ_R is normalized by Γ_{R0} defined by Eq. (11). Figures 25 and 26 also show the mean concentrations of reactive species in the frozen limit (Eqs. (12) and (13)) and the equilibrium limit (Eqs. (15), (16), and (17)). The mean concentration of reactant species A involved in the jet flow is smaller than the frozen limit owing to consumption by the chemical reaction. Similarly, the mean concentration of reactant species B involved in the main flow is smaller than the frozen limit. The differences between the mean concentrations of reactant species and those in the frozen limit increase in the downstream direction because the chemical reaction proceeds in the downstream direction. Γ_A/Γ_{A0} on the jet

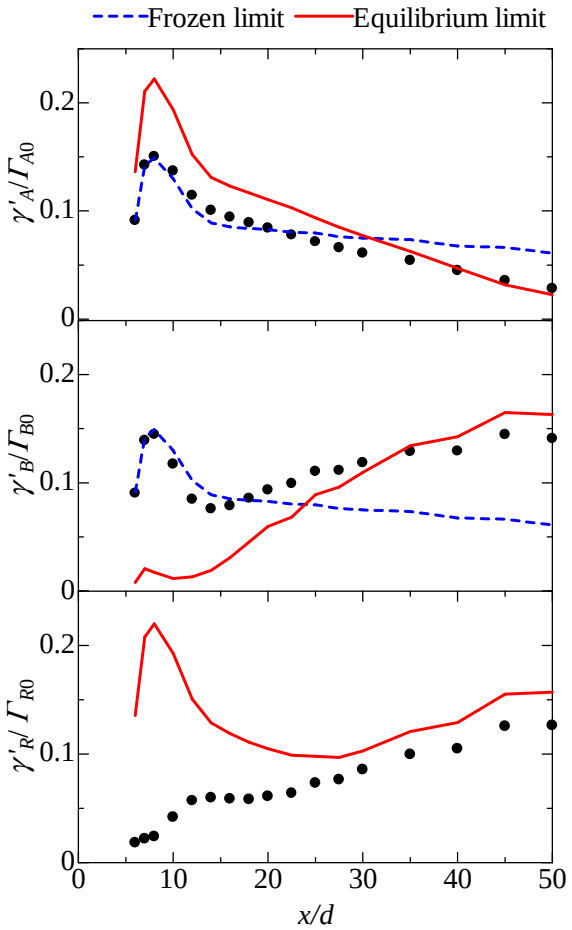

Fig. 27 The streamwise evolution of the rms value of concentration fluctuation of reactive species.

centerline decreases in the downstream direction owing to turbulent diffusion and the chemical reaction. By contrast, Γ_B/Γ_{B0} on the jet centerline decreases in the downstream direction owing to the chemical reaction and increases in the downstream direction owing to turbulent diffusion. Hence, the streamwise evolution of Γ_B/Γ_{B0} is complicated in comparison with that of species A. In Fig. 25, Γ_B/Γ_{B0} increases in the downstream direction in the region $6 \leq x/d \leq 12$ because in this region the increment of species B arising from turbulent diffusion exceeds the decrement of species B arising from the chemical reaction. In the region $12 \leq x/d \leq 25$, Γ_B/Γ_{B0} decreases in the downstream direction. This is because the decrement of species B owing to the chemical reaction exceeds the increment of species B owing to turbulent diffusion in this region. In the further downstream region $25 \leq x/d \leq 50$, Γ_B/Γ_{B0} increases again in

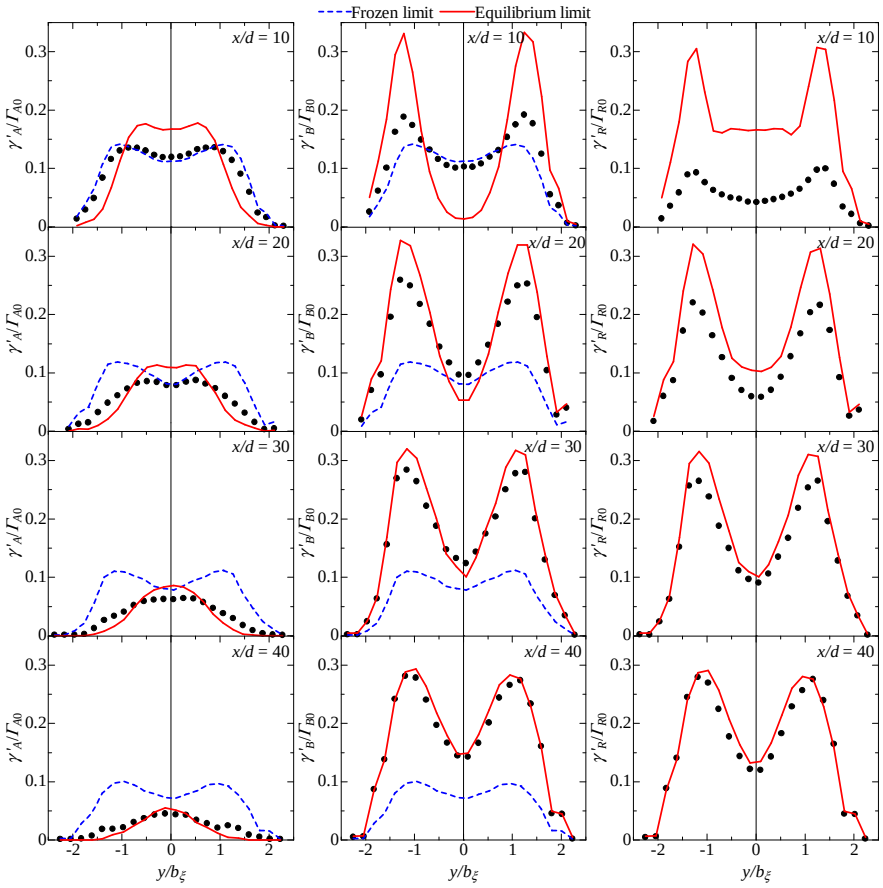

Fig. 28 Lateral profiles of the rms value of concentration fluctuation of reactive species.

the downstream direction. In this region, the reaction rate is very small because most of species A, one of the reactant species, has already reacted. Hence, Γ_B/Γ_{B0} increases in the downstream direction owing to turbulent diffusion in the region $25 \leq x/d \leq 50$. Figure 25 shows that Γ_R/Γ_{R0} on the jet centerline increases mainly in the region $10 \leq x/d \leq 25$ where the chemical reaction proceeds rapidly and increases gradually in the region of $25 \leq x/d \leq 50$ where the chemical reaction rate is small owing to the small concentration of species A. Figure 26 shows that Γ_R/Γ_{R0} has peak values near the half-width of the mixture fraction in the region near the jet exit, whereas in the downstream region Γ_R/Γ_{R0} has a peak value on the jet centerline.

Bilger et al. (1991) have shown that the mean concentration of reactive species lies between concentrations for the frozen and equilibrium limits as for the instantaneous reactive concentration. In Figs. 25 and 26, it is confirmed that mean concentrations measured in this study satisfy this relationship.

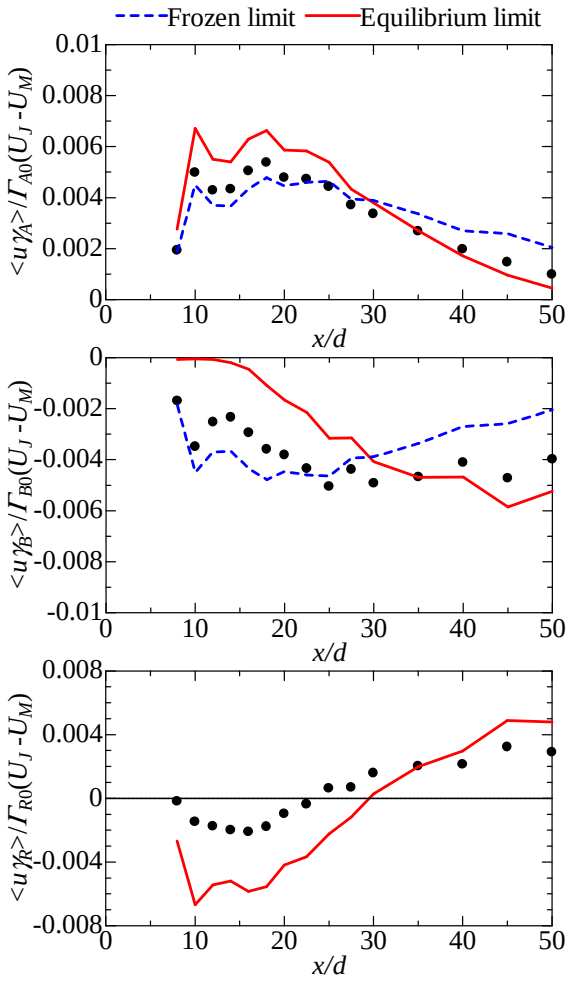

Fig. 29 The streamwise evolution of the streamwise turbulent mass fluxes.

Figure 27 shows the streamwise evolution of the rms values of concentration fluctuation of reactive species γ_i' (i = A, B, or R) on the jet centerline and Fig. 28 shows the lateral profiles of γ_i'. In Figs. 27 and 28, γ_A' and γ_B' are normalized by the respective initial concentrations and γ_R' is normalized by Γ_{R0}. The influence of the chemical reaction on the rms value of reactant species is different between the region near the jet exit and the other region (e.g., the outer edge of the flow and the downstream region). γ_A'/Γ_{A0} is larger than the frozen limit near the jet exit whereas in the other region it is smaller than the frozen limit. By contrast, γ_B'/Γ_{B0} is smaller than the frozen limit near the jet exit whereas it is larger than the frozen limit in the other region. The difference between the rms values of concentration fluctuation of reactant

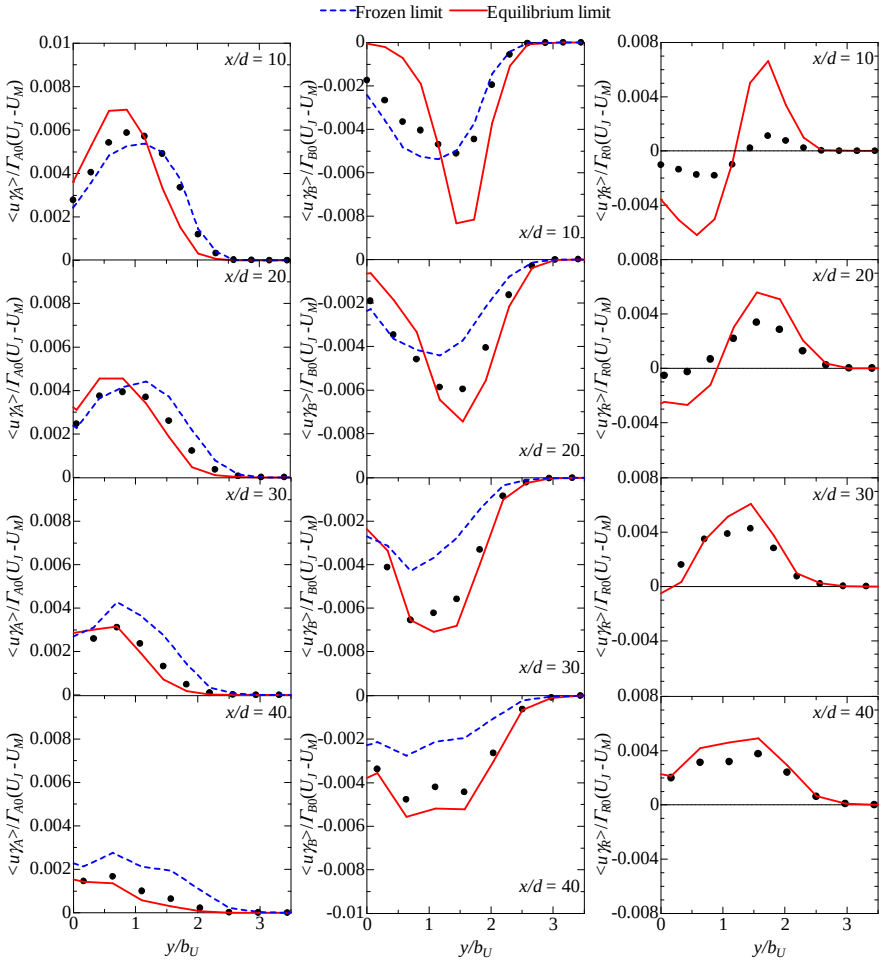

Fig. 30 Lateral profiles of the streamwise turbulent mass fluxes.

species and that for the frozen limit is large in the slightly outer region of the half-width of the mixture fraction.

γ'_R/Γ_{R0} increases mainly in the region $8 \leq x/d \leq 12$ and is nearly constant in the region $12 \leq x/d \leq 20$. In the further downstream region, γ'_R/Γ_{R0} increases gradually. Figure 28 shows that γ'_R/Γ_{R0} has peak values in the slightly outer region of the half-width of the mixture fraction.

Figure 29 shows the streamwise evolution of the streamwise turbulent mass fluxes of reactive species $\langle u\gamma_i \rangle$ (i = A, B, or R) on the jet centerline and Fig. 30 shows the lateral profiles of $\langle u\gamma_i \rangle$. In these figures, $\langle u\gamma_i \rangle$ is normalized by Γ_{i0} and $(U_J - U_M)$, and the abscissa is normalized by the slit width d or the velocity half-width b_U. In a similar way to γ'_i/Γ_{i0}, the influence of chemical reaction on the turbulent mass flux of reactive species is different between

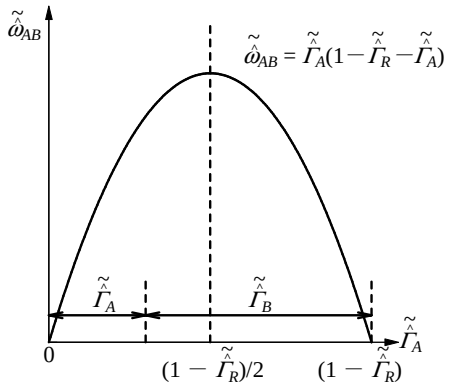

Fig. 31 The variation of chemical reaction rate with the concentration of reactant species A.

the region near the jet exit and the other region. The turbulent mass flux of reactant species A is larger than the frozen limit near the jet exit and is smaller than the frozen limit in the other region. By contrast, the magnitude of turbulent mass flux of reactant species B is smaller (closer to zero) than the frozen limit near the jet exit and is larger than the frozen limit in the other region. Note that the turbulent mass flux of reactant species B shows a negative value. The turbulent mass flux of product species R has a negative value near the jet exit whereas it has a positive value in the other region.

The reason for the different influence of chemical reaction on the rms value and the turbulent mass flux of reactive species between the region near the jet exit and the other region is explained by the conservation law of Eq. (10) and the dependency of the instantaneous reaction rate on the instantaneous concentration of the reactant species. The reaction rate of this second-order chemical reaction is proportional to the product of normalized concentrations of reactant species A and B, denoted by $\tilde{\hat{\omega}}_{AB}$. Here, the caret ($\hat{}$) denotes the normalized value. Using Eq. (10), we can represent $\tilde{\hat{\omega}}_{AB}$ as follows:

$$\begin{aligned}\tilde{\hat{\omega}}_{AB} &= \tilde{\hat{\Gamma}}_A\tilde{\hat{\Gamma}}_B \\ &= \tilde{\hat{\Gamma}}_A(1-\tilde{\hat{\Gamma}}_R-\tilde{\hat{\Gamma}}_A) = -\{\tilde{\hat{\Gamma}}_A-\frac{1}{2}(1-\tilde{\hat{\Gamma}}_R)\}^2+\frac{1}{4}(1-\tilde{\hat{\Gamma}}_R)^2 \quad (19)\\ &= \tilde{\hat{\Gamma}}_B(1-\tilde{\hat{\Gamma}}_R-\tilde{\hat{\Gamma}}_B) = -\{\tilde{\hat{\Gamma}}_B-\frac{1}{2}(1-\tilde{\hat{\Gamma}}_R)\}^2+\frac{1}{4}(1-\tilde{\hat{\Gamma}}_R)^2, \quad (20)\end{aligned}$$

where $\tilde{\hat{\Gamma}}_i = \tilde{\Gamma}_i/\Gamma_{i0}$ (i = A, B, or R). Thus, $\tilde{\hat{\omega}}_{AB}$ is a quadratic function of $\tilde{\hat{\Gamma}}_A$(and $\tilde{\hat{\Gamma}}_B$). As shown in Fig. 31, Eqs. (19) and (20) imply that the reaction rate becomes maximum on the condition $\tilde{\hat{\Gamma}}_A = \tilde{\hat{\Gamma}}_B = (1-\tilde{\hat{\Gamma}}_R)/2$. Near the jet exit, the concentration of species A (the contaminant in the jet flow), $\tilde{\hat{\Gamma}}_A$, is larger than the concentration of species B (the contaminant in the main flow), $\tilde{\hat{\Gamma}}_B$: therefore, $\tilde{\hat{\Gamma}}_A > (1-\tilde{\hat{\Gamma}}_R)/2$. From Eqs. (19) and (20), near the jet exit, when

$\tilde{\hat{\Gamma}}_A$ becomes small and $\tilde{\hat{\Gamma}}_B$ becomes large, the reaction rate becomes large. Therefore, the consumption of reactant species by the chemical reaction, which occurs when the reaction rate become large, makes the negative fluctuation of species A large and the positive fluctuation of species B small. Thus, the rms value of concentration fluctuation of species A is larger than the frozen limit and that of species B is smaller than the frozen limit near the jet exit. Similarly, the turbulent mass flux of species A is larger than the frozen limit and that of species B is close to zero compared with the frozen limit owing to the chemical reaction. When the reaction rate is large, the fluctuation of species R has a positive value. Near the jet exit, a large reaction rate corresponds to a negative fluctuation of species A and a positive fluctuation of species B as discussed above. In consideration of the correlation between γ_i and u, this means that the turbulent mass flux of product species R has the same sign as that of species B in this region. As a result, the turbulent mass flux of product species R has a negative value near the jet exit.

In the other region, the concentration of species A, $\tilde{\hat{\Gamma}}_A$, is smaller than that of species B, $\tilde{\hat{\Gamma}}_B$. Therefore, from Eqs. (19) and (20), it is found that, when $\tilde{\hat{\Gamma}}_A$ is large and $\tilde{\hat{\Gamma}}_B$ is small, the reaction rate becomes large in this region. This is opposite to the trend in the region near the jet exit. This difference leads to differing influences of the chemical reaction on the rms value and the turbulent mass flux of reactive species near the jet exit and that in the other region.

Bilger et al. (1991) and Komori et al. (1993) have measured the rms value of reactant concentration fluctuation and the turbulent flux of reactant species in the scalar mixing layer. Their results show that the rms value of concentration fluctuation and the turbulent mass flux of the reactant species are made large by the chemical reaction in the region where the reactant species is abundant, whereas the rms value of concentration fluctuation and the turbulent mass flux of the deficient reactant species become small. The same tendencies are also found in the present planar liquid jet as shown in Figs. 27–30. Brown and Bilger (1996) have measured the rms value of reactant concentration fluctuation and the turbulent flux of reactant species in a plume in grid turbulence, and have shown that the rms value of concentration fluctuation and the turbulent mass flux of the reactant species premixed in the plume always behave as the deficient species whereas those of the reactant species premixed in the ambient always behave as the abundant reactant. In Figs. 27–30, it is found that the reactants premixed into the jet and the main flow can be both the abundant and deficient species in a planar liquid jet.

4 Conclusions

This paper described a new experimental method for simultaneous measurements of instantaneous velocity and concentrations of reactive species by combining I-type hot-film anemometry with light absorption spectrometry. This

method is applied to investigate a planar liquid jet with a second-order chemical reaction ($A + B \rightarrow R$). The main results of this paper are summarized as follows.

1. A combined probe, which consists of an I-type hot-film probe and an optical fiber probe based on light absorption spectrometry, has been developed. It is confirmed that it is possible to simultaneously measure streamwise velocity and concentration using the combined probe.
2. The mean concentrations of reactant species A and B are smaller than the frozen limit corresponding to the limiting case of no chemical reaction. The mean concentration of product species R increases in the downstream direction.
3. The rms value of concentration fluctuation of species A is larger than the frozen limit near the jet exit and smaller than the frozen limit in the other region (e.g., the outer region of the jet and the downstream region). In contrast, the rms value of concentration fluctuation of species B is smaller than the frozen limit near the jet exit and larger than the frozen limit in the other region.
4. The turbulent mass flux of species A is positive and larger than the frozen limit near the jet exit and smaller than the frozen limit in the other region, whereas that of species B is negative and its magnitude is close to zero near the jet exit and larger than the frozen limit in the other region. For the product species R, the turbulent mass flux has a negative value near the jet exit and a positive value in the other region.
5. The influence of the chemical reaction on the rms value and the turbulent mass flux of concentration fluctuation of reactive species is different between the region near the jet exit and the other region. This difference arises from the dependency of instantaneous reaction rate on the instantaneous concentration of reactive species.

Acknowledgements This work was supported by Grants-in-Aid for Scientific Research Nos. 22360077, 23656133, and 23656134. The authors thank Mr. Hiroki Yasuhara for his help in conducting experiments.

References

Bennani A, Gence JN, Mathieu J (1985) The influence of a grid-generated turbulence on the development of chemical reactions. AIChE Journal 31(7):1157–1166

Bilger RW, Saetran LR, Krishnamoorthy LV (1991) Reaction in a scalar mixing layer. Journal of Fluid Mechanics 233:211–242

Borg A, Bolinder J, Fuchs L (2001) Simultaneous velocity and concentration measurements in the near field of a turbulent low-pressure jet by digital particle image velocimetry–planar laser-induced fluorescence. Experiments in Fluids 31(2):140–152

Bourne JR, Hilber C, Tovstiga G (1985) Kinetics of the azo coupling reactions between 1-naphthol and diazotised sulphanilic acid. Chemical Engineering Communications 37(1):293–314

Brown RJ, Bilger RW (1996) An experimental study of a reactive plume in grid turbulence. Journal of Fluid Mechanics 312:373–407

Feng H, Olsen MG, Hill JC, Fox RO (2007) Simultaneous velocity and concentration field measurements of passive-scalar mixing in a confined rectangular jet. Experiments in fluids 42(6):847–862

Feng H, Olsen MG, Hill JC, Fox RO (2010) Investigation of passive scalar mixing in a confined rectangular wake using simultaneous PIV and PLIF. Chemical Engineering Science 65(11):3372–3383

Hu H, Saga T, Kobayashi T, Taniguchi N (2004) Analysis of a turbulent jet mixing flow by using a PIV-PLIF combined system. Journal of visualization 7(1):33–42

Komori S, Nagata K, Kanzaki T, Murakami Y (1993) Measurements of mass flux in a turbulent liquid flow with a chemical reaction. AIChE Journal 39(10):1611–1620

Komori S, Kanzaki T, Murakami Y (1994) Concentration correlation in a turbulent mixing layer with chemical reactions. Journal of Chemical Engineering of Japan 27(6):742–748

Kubo T, Sakai Y, Nagata K, Iida K (2009) Experimental study on the turbulent reactive plane jet in liquid. Journal of Fluid Science and Technology 4(2):368–378

Lee J, Brodkey RS (1964) Turbulent motion and mixing in a pipe. AIChE Journal 10(2):187–193

Li JD, Bilger RW (1996) The diffusion of conserved and reactive scalars behind line sources in homogeneous turbulence. Journal of Fluid Mechanics 318:339–372

Madhani JT, Brown RJ (2008) A scalar concentration (Komori) probe for measuring fluctuating dye concentration in water. WSEAS Transactions on Fluid Mechanics (special issue on" Energy and Environmental Fluid Mechanics) 3(3):224–233

Mehta RV, Tarbell JM (1987) An experimental study of the effect of turbulent mixing on the selectivity of competing reactions. AIChE Journal 33(7):1089–1101

Nakamura I, Sakai Y, Miyata M (1987) Diffusion of matter by a non-buoyant plume in grid-generated turbulence. Journal of Fluid Mechanics 178(-1):379–403

Sakai Y, Nakamura I, Kubo T (1997) An experimental study on the consecutive and competing reaction in a turbulent liquid jet by the light absorption spectrometric method. Proceedings of the 11th Symposium on Turbulent Shear Flows (Grenoble, France) 2(18):19–24

Sakai Y, Okada Y, Kobayashi N, Nakamura I, Miwa M (1999) Measurements of velocity-scalar joint statistics in a high Schmidt number axisymmetric turbulent jet. In: Proceedings of the Third ASME/JSME Joint Fluids Engineering Conference, San Francisco, paper, pp 1–8

Su LK, Mungal MG (2004) Simultaneous measurements of scalar and velocity field evolution in turbulent crossflowing jets. Journal of fluid mechanics 513:1–45

Webster DR, Roberts PJW, Ra'ad L (2001) Simultaneous DPTV/PLIF measurements of a turbulent jet. Experiments in Fluids 30(1):65–72